INDONESIAN JOURNAL ON GEOSCIENCE
Geological Agency
Ministry of Energy and Mineral Resources

Journal homepage: http://ijog.geologi.esdm.go.id
ISSN 2355-9314, e-ISSN 2355-9306

# Uneven Land Subsidence Patterns Along Java's Northern Urban Corridor (Pantura Route) from 2.5D SBAS InSAR Approach

Afif Janur[1], Harintaka[2], and Argo Galih Suhadha[3]

[1]Master of Geomatic Study Programme, Faculty of Engineering, Universitas Gadjah Mada, Sleman, Indonesia
[2]Department of Geodetic Engineering, Faculty of Engineering, Universitas Gadjah Mada, Sleman, Indonesia
[3]Research Center for Geoinformatics, National Research and Innovation Agency (BRIN), Bandung, Indonesia

Corresponding author: harintaka@ugm.ac.id
Manuscript received: April, 04, 2024; revised: December, 05, 2024;
approved: August, 13, 2025; available online: August, 29, 2025

**Abstract -** Land subsidence is a phenomenon that occurs in many parts of the world, particularly in coastal plains and river delta areas, including the north coast of Java, commonly known as 'pantura'. By utilizing satellite time series data, land subsidence along the north coast of Java was detected using The Small Baseline Subset (SBAS) method. Additionally, combining data from different Sentinel-1 orbit directions (ascending-descending) enables the production of a more accurate 2.5D model. This research aims to calculate the rate of land subsidence on the north coast of Java from 2020 to 2023 using the 2.5D model, and to compare the results with CORS processing results. Recent identification of land subsidence highlights that residential areas and rice fields are highly vulnerable to potential subsidence. The 2.5D model in the up-down (UD) direction shows the highest land subsidence occurred in Demak Regency at 146.45 mm/year, Semarang City at 144.34 mm/year, and Pekalongan Regency at 137.94 mm/year. An accuracy assessment was performed using twelve CORS stations, showing RMSE values ranging from millimeters to centimeters: vertical ascending at 16.5 mm, vertical descending at 18.6 mm, UD at 8.8 mm, and East–West (EW) at 26.3 mm.

**Keywords**: InSAR, CORS, Land Subsidence, 2.5D Model, *pantura*



**How to cite this article:**
Janur, A., Harintaka, and Suhadha, A.G., 2025. Uneven Land Subsidence Patterns Along Java Northern Urban Corridor (Pantura Route) from 2.5D SBAS InSAR Approach. *Indonesian Journal on Geoscience*, 12 (2), p.281-300. DOI:10.17014/ ijog.12.2.281-300

## Introduction

### Background

Land subsidence is the gradual or sudden lowering of the ground surface in a particular segment (Galloway and Burbey, 2011). This phenomenon results from both natural and human-induced factors, including compaction, exploitation of natural resources, ice sheet degradation, peatland burning, land drainage, and urbanization (Huning *et al*., 2024). Land subsidence can lead to severe consequences, such as infrastructure damage, increased flood risk, and reduced aquifer storage capacity (Davydzenka *et al*., 2024). This global issue is particularly prevalent in coastal plains and river delta regions. According to Gavkosh *et al*. (2021), 47b% of 290 researched areas worldwide report significant subsidence, with coastal plains and deltaic areas being the most affected. A prominent example is Indonesia north coast of Java, also known as "Pantura." Pantura refers to the route that runs parallel to the coastline in the northern part of Java Island. This research focuses on cities that are located along the pantura route.

The north coast of Java holds vital economic importance, serving as the hub for various eco-

nomic activities in Indonesia (Yulianto *et al*., 2023). It is not a singular administrative region, but rather a collection of regencies and cities situated along the coast, and directly adjacent to The Java Sea (Suroso and Firman, 2018). Several studies have observed land subsidence in these areas, including Jakarta, Bekasi (Wu *et al*., 2022; Harintaka *et al*., 2024), Cirebon (Bramanto *et al*., 2023), Pekalongan (Sarah *et al*., 2021), Semarang (*Sarah et al*., 2020; Widada *et al*., 2020; Takami, 2021; Parwata *et al*., 2023), Demak (Sarah *et al*., 2020), and Surabaya (Anjasmara *et al*., 2020). Monitoring subsidence along the north coast of Java can be effectively achieved using GNSS (Susilo *et al*., 2023) and InSAR (Ardha *et al*., 2022). InSAR, in particular, is well-suited for large-scale monitoring, making it ideal for regions like the north coast of Java.

Advancements in satellite technology have made it possible to observe land subsidence using Interferometric Synthetic Aperture Radar (InSAR). This technique measures ground deformation by analyzing phase differences in radar signals (Castañeda *et al*., 2011). A key variation of this approach, Differential InSAR (DInSAR), calculates deformation by comparing two radar interferograms (Ren *et al*., 2019). However, the use of the DInSAR method also still has limitations due to spatial temporal decorrelation and atmospheric delay, which impacts on the accuracy of DInSAR measurement results (Lanari *et al*., 2020; Bassols *et al*., 2021; Zhang *et al*., 2023). The problems with the DInSAR method can be overcome by using tens or even hundreds of SAR images observed over a very long time known as Time-Series InSAR (TS-InSAR) (Zhang *et al*., 2023).

Persistent Scatterer InSAR (PS-InSAR), the first TS-InSAR method, is used to identify permanent points with high coherence on man-made structures, rocks and urban areas *(*Wu *et al*., 2023). In the low-coherence suburbs, PS-InSAR cannot deal with rural and vegetation areas. To address this, Small Baseline Subset (SBAS) was developed (Wu *et al*., 2023). SBAS can overcome the weakness of the PS-InSAR method to observe broader areas. The development of TS-InSAR methods has posed challenges in processing large datasets for specific applications. LiCSBAS is an open-source software developed by Morishita *et al*. (2020) that allows users to bypass the generation of interferograms. Therefore, users can get time-series deformation analysis results quickly, easily, and do not require a high-end computer.

LiCSBAS processing results in the form of Line of Sight (LOS) displacement in 1D. However, ground deformation processes occur in three dimensions, namely east -west (EW), north - south (NS), and up-downward (UD) (Ding *et al*., 2004). In reality, Sentinel-1A only provides ascending and descending orbits, preventing 3D modelling. When SAR observations from multiple orbital paths (ascending and descending) are available, it is possible to combine LOS to produce a 2.5D model (Fujiwara *et al*., 2000). Based on these developments, it is necessary to combine multiorbital SAR data pairs (ascending-descending) to increase the result of vertical displacement due to the differentiating with the horizontal. This study aims to map the current land subsidence locations on the north coast of Java and their displacement rate from 2020 to 2023 using a 2.5D model, validated with the results of GNSS CORS data.

**Geological/Stratigraphical Settings**

Java Island is located at the convergence of The Eurasian Plate and The Indo-Australian Plate (Schlüter *et al*., 2002; Metcalfe, 2011; Pasari *et al*., 2021). The plate meeting results in the subduction process of The Indo-Australian Plate under The Eurasian Plate (Hammond *et al.*, 2010). In the southern part of Java, a volcanic rock has formed due to subduction, while the northern part of Java experiences less intense volcanic activity, and is instead dominated by fault structures (Novico *et al*., 2022).

According to The Indonesian National Centre for Earthquake Studies, several faults are located in the *pantura* region, including the Subang, Cirebon, Cirebon-1, Cirebon-2, Brebes, Tegal, Pema-

lang, Pekalongan, Weleri, Semarang, Ungaran-1, Ungaran-2, Demak, Muria, Pati, Blumbang, Waru, Surabaya, Pasuruan, and Probolinggo faults. The distribution of locations can be seen in Figure 1.

Figure 2 shows the modified geological formation map of the coastal area, adapted from The Ministry of Energy and Mineral Resources of The Republic of Indonesia. Based on the distribution of Pantura geological formations, there are five formations that have the highest area compared to other formations. The formations consist of Alluvium of 10,933 km$^2$, Flood Plain Deposits of 2,391 km$^2$, Upper Banten Tuff of 1,169 km$^2$, Muria Tuff of 1,042 km$^2$, and Argopuro Volcanics of 858 km$^2$.

Visually, the Alluvium Formations are distributed almost continuously along the north coast of Java, while the other formations are only limited to certain areas. The Alluvium Formation consists of gravel, sand, silt, and mud, while the Argopuro Volcanics Formation comprises andesite to basaltic lavas, volcanic breccia, and volcanic debris. The Flood Plain Deposit Formation is

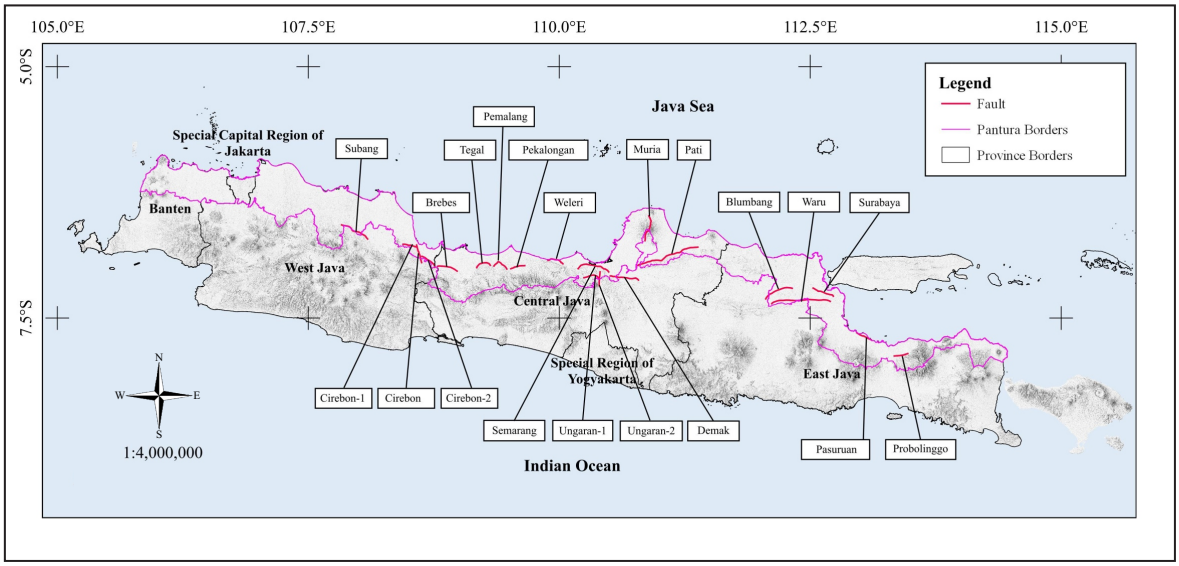


Figure 1. Location of faults in Pantura.

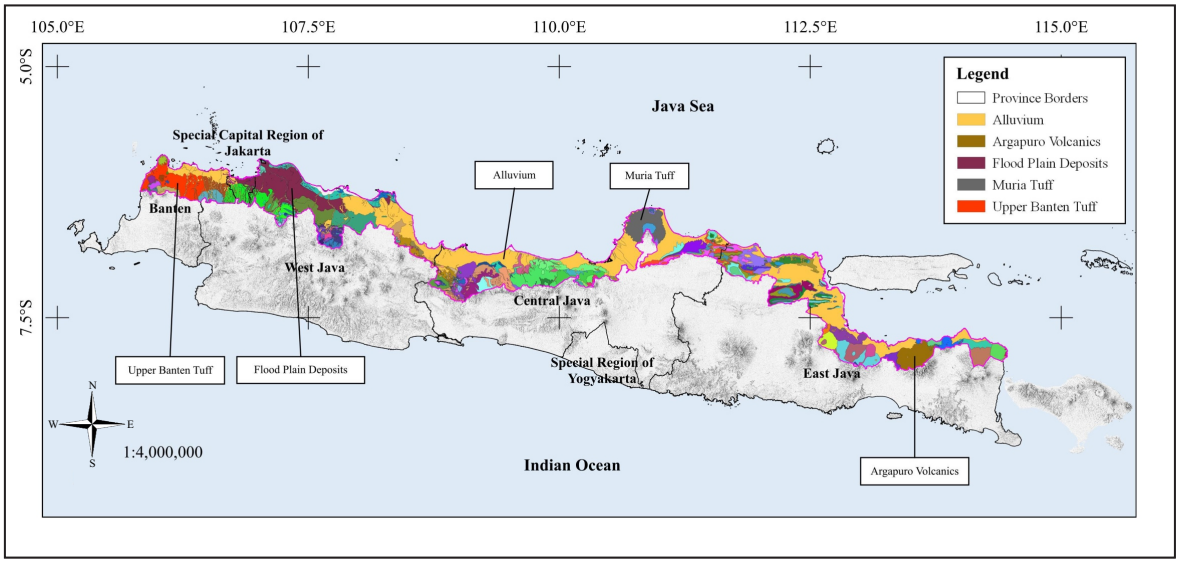


Figure 2. Geological formations in Pantura.

composed of clayey sand, sand clay, and peaty clay. Additionaly, The Muria Tuff Formation consists of tuff, lahar, and sandy tuff, while The Upper Banten Tuff Formation consists of tuff, pumiceous tuff, and tuffaceous standstone.

## Methods and Materials

### Methods

*LiCSBAS*

LiCSBAS is an open-source software designed for a time series InSAR analysis, developed by Morishita *et al*. (2020). One of its key advantages is that users do not need to process and generate interferograms. LiCSBAS calculates the velocity of the surface pixels over time based on displacement dataset using the Small Baseline Inversion (SBI) technique (Morishita *et al*., 2020). SBI is a technique for analyzing the deformation of the earth's surface by utilizing pairs of radar images with narrow or small baselines. However, the drawbacks of SBI are the possibility of gaps in the data mesh (due to vegetation and snow cover), large acquisition gaps between frames, and pixel-by-pixel errors in the image (Morishita *et al*., 2020).

To overcome these limitations, The Narrow Baseline Subset (NBAS) approach is used. NBAS is a method in which only radar image pairs with narrow or small baselines are selected for further analysis (Morishita *et al*., 2020). By limiting the temporal constraint, NBAS can address the problem of data gaps, and prevent the calculated displacement from becoming zero. Thus, providing a more accurate representation of the earth surface deformation *(*Morishita *et al*., 2020). Therefore, NBAS is a solution to improve the accuracy and reliability of surface deformation analysis using radar interferometry data. Despite its advantages, LiCSBAS has some limitations. For instance, the interferogram produced by LiCSAR has a spatial resolution of up to 100 m, making it less suitable for monitoring more localized deformations, such as infrastructure stability monitoring.

*Model 2.5D*

In recent decades, InSAR has proven to be a reliable technique for detecting and measuring ground movements over large areas with high spatial resolution (Fuhrmann and Garthwaite, 2019). However, one key limitation of InSAR is that its measurements are still confined to one dimension, commonly referred as The Line of Sight (LOS). LOS represents the direct distance from the radar antenna to the target on earth surface, and is critical for projecting movement in the upward-downward (UD) direction (Fuhrmann and Garthwaite, 2019; Suhadha and Harintaka, 2024).

$$UD = \frac{LOS}{\cos\theta} \quad \text{..... (1)}$$

The UD projection from one orbit only yields one-dimensional movement. In reality, earth crustal movement occurs in three dimensions: east -west (EW), north -south (NS), and up -down (UD) (Fuhrmann and Garthwaite, 2019). This implies that InSAR cannot fully depict the magnitude and direction of the surface features. To overcome this limitation, measurements from two or more LOS geometries can be combined to generate vertical and horizontal components (Fuhrmann and Garthwaite, 2019).

This condition can be met if LOS measurements are available at the same location and during the same time period. To create a 3D model (EW, NS, UD), two ascending orbits and two descending orbits are required to apply least-squares adjustment (LSA) to the interpolated line-of-sight (LOS) velocities (observation vector y). Thus, solving for velocities in the E, N, and U directions (unknown parameter x) (Fuhrmann and Garthwaite, 2019).

$$y = A.x + e \quad \text{..... (2)}$$

$$\begin{matrix} LOS_{asc1} \\ LOS_{asc2} \\ LOS_{des1} \\ LOS_{des2} \end{matrix} = \begin{pmatrix} -\sin\theta_{asc1}\cos\alpha_{asc1} & -\sin\theta_{asc1}\sin\alpha_{asc1} & \cos\alpha_{asc1} \\ -\sin\theta_{asc2}\cos\alpha_{asc2} & -\sin\theta_{asc2}\sin\alpha_{asc2} & \cos\alpha_{asc2} \\ -\sin\theta_{des1}\cos\alpha_{des1} & -\sin\theta_{des1}\sin\alpha_{des1} & \cos\alpha_{des1} \\ -\sin\theta_{des2}\cos\alpha_{des2} & -\sin\theta_{des2}\sin\alpha_{des2} & \cos\alpha_{des2} \end{pmatrix} \begin{pmatrix} v_{ew} \\ v_{ns} \\ v_{UD} \end{pmatrix} + e \quad \text{.. (3)}$$

In fact, Sentinel-1A only provides ascending and descending orbits, it is not possible to solve the full 3D model. Therefore, the NS direction is assumed to be zero to simplify the equation (Fuhrmann and Garthwaite, 2019). The model generated from this equation is a 2.5D model, which only shows movement directions in the easting and upward directions (Fuhrmann and Garthwaite, 2019; Fujiwara *et al.*, 2000).

$$\begin{pmatrix} LOS_{asc} \\ LOS_{des} \end{pmatrix} = \begin{pmatrix} -\sin\theta_{asc}\cos\alpha_{asc}\cos\theta_{asc} \\ LOS_{des}\cos\alpha_{des}\cos\theta_{des} \end{pmatrix} \begin{pmatrix} v_{ew} \\ v_{UD} \end{pmatrix} \quad \text{..... (4)}$$

*PPP-Pride*

PPP Pride-AR is an open-source software developed by Pride Lab at the GNSS Research Center, Wuhan University. It follows principles of readability, modularity, and extensibility in GNSS data processing (Geng *et al.*, 2019). PPP Pride-AR was developed using the FORTRAN-95 programming language, which is well-suited for numerical and scientific calculations, providing strong advantages in data processing (Geng *et al.*, 2019). It follows principles of readability, modularity, and extensibility in GNSS data processing.

The processing of PPP Pride-AR consists of two main modules, namely undifferenced GPS data processing and integer ambiguity resolution (Geng *et al.*, 2019). The undifferenced GPS data processing module consists of two functions: data cleaning, which estimates unknown parameters such as position, receiver clock, tropospheric delay, and ambiguity Y. This module produces float ambiguity solutions (Geng *et al.*, 2019). These results will be used as input data for the integer ambiguity resolution module (Geng *et al.*, 2019).

In the ambiguity resolution module, the phase a biased clock product from Pride Lab is used to restore undifferenced ambiguity into an integer form (Geng *et al.*, 2019). These final results include a file containing daily shifts (x, y, z), which are used to determine the velocity of each CORS station.

## Materials

Frame ID identification was performed using the COMET-LiCS portal, which provides unwrapping and coherence data processed automatically by LiCSAR. Available frame IDs are marked by frames distributed across several regions. This distribution occur, because LiCSAR is only intended to monitor areas actively experiencing ground movement, earthquakes, tectonic plate movements, and volcanic activity.

In Figure 3, ascending orbit is marked in green, while descending in blue. These frames

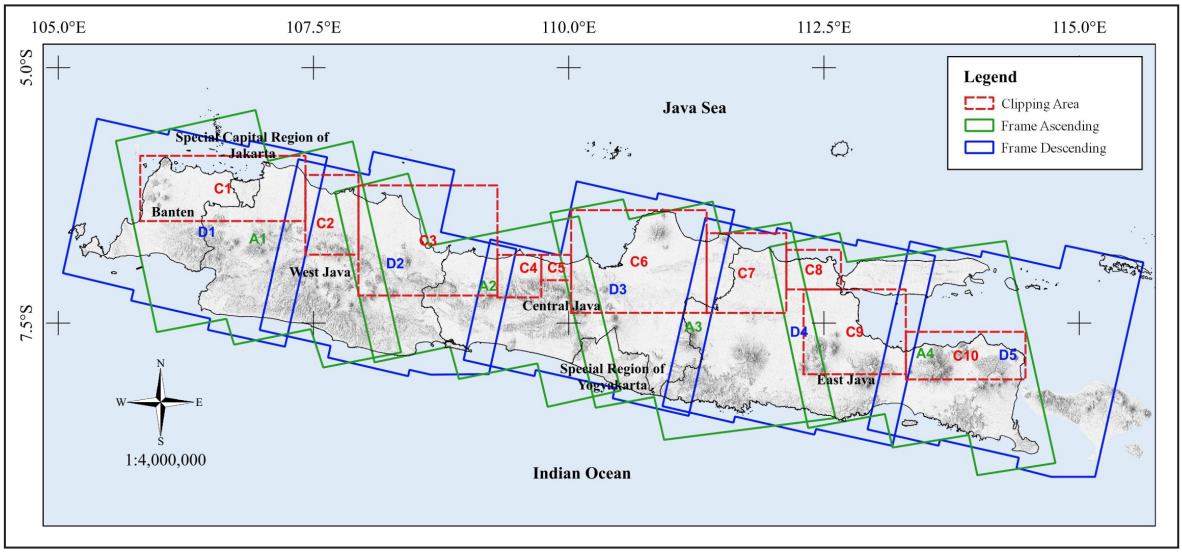


Figure 3. Overlay frame ID orbit ascending, frame ID orbit descending, and clipping image.

cover the entire Java Island, but this study only focuses in *pantura*. To optimize the data processing, image cropping was performed to produce a clip of the studied area (marked in red). Table 1 lists the ascending and descending LiCSAR frame IDs used for these clip areas. It is important to note that overlapping ascending and descending frames are necessary to generate a 2.5D image model. If no overlap occurs, the 2.5D model cannot be produced.

Figure 4 shows the locations of the CORS stations used to validate the LiCSBAS processing results. The selection of CORS stations is based on the overlap between pixels and the CORS station positions. Therefore, some CORS stations were excluded. As shown in Table 2, there are twelve CORS stations used in this study. In Banten Province, there is one CORS station, West Java has one CORS station, Central Java has four CORS stations, and East Java has six CORS stations. For Jakarta, there are no CORS stations used due to the absence of pixels from LiCSBAS processing.

Table 1. Description of frame's ID of Sentinel-1

| Frame ID Ascending | Frame ID Descending | Clip |
|---|---|---|
| 098A_09673_121312 (A1) | 047D_09652_111009 (D1) | Clip 1 |
| 098A_09673_121312 (A1) | 149D_09700_081210 (D2) | Clip 2 |
| 025A_09718_120810 (A2) | 149D_09700_081210 (D2) | Clip 3 |
| 025A_09718_120810 (A2) | 076D_09725_121107 (D3) | Clip 4 |
| 025A_09718_120810 (A2) | 076D_09725_121107 (D3) | Clip 5 |
| 127A_09749_121312 (A3) | 076D_09725_121107 (D3) | Clip 6 |
| 127A_09749_121312 (A3) | 003D_09757_111111 (D4) | Clip 7 |
| 054A_09773_111213 (A4) | 003D_09757_111111 (D4) | Clip 8 |
| 054A_09773_111213 (A4) | 003D_09757_111111 (D4) | Clip 9 |
| 054A_09773_111213 (A4) | 105D_09782_131111 (D5) | Clip 10 |

## Result and Discussion

### 1D Asc, Des, and 2.5D Displacement Velocities

The velocity results from LiCSBAS processing, both ascending and descending, are initially expressed in the LOS direction. Therefore, LOS conversion was performed to obtain the vertical displacement. Based on Harintaka *et al*. (2024), it is recommended to combine the SAR data pairs from multi-orbit (ascending-descending) to increase the shifting that occurs, to produce 2.5D models in the EW and UD directions. The velocity results in the vertical ascending, vertical descending, UD, and EW directions will be used to identify land subsidence along the north coast of Java.

Figure 5 shows the results of the vertical ascending, vertical descending, 2.5D model in UD direction, and 2.5D model in EW direction in *pantura*. Visual analysis indicates that vertical ascending and vertical descending results have similar land subsidence locations. The 2.5D

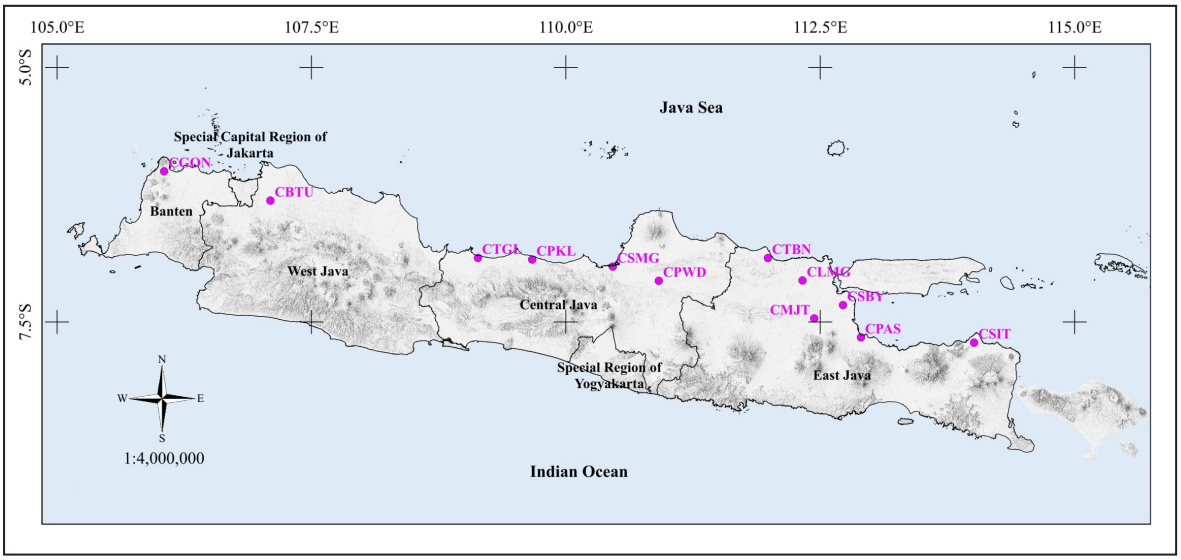


Figure 4. Location of CORS stations.

Table 2. Description of CORS Stations

| Name | Longitude | Latitude | Location | Province |
|---|---|---|---|---|
| CGON | -6.02077 | 106.0522 | Jombang, Cilegon | Banten |
| CBTU | -6.30832 | 107.0964 | Cibitung, Bekasi | West Java |
| CTGL | -6.87119 | 109.1361 | Tegal, Tegal | Central Java |
| CPKL | -6.88701 | 109.6694 | Pekalongan, Pekalongan | |
| CSEM | -6.987269 | 110.37693 | Kalibanteng, Semarang | |
| CPWD | -7.09608 | 110.9142 | Purwodadi, Grobogan | |
| CTBN | -6.87225 | 111.9864 | Merakurak, Tuban | East Java |
| CLMG | -7.0926 | 112.3265 | Sukodadi, Lamongan | |
| CSBY | -7.33434 | 112.7244 | Gayungan, Surabaya | |
| CMJT | -7.46558 | 112.4416 | Magersari, Mojokerto | |
| CPAS | -7.65141 | 112.901 | Purworejo, Pasuruan | |
| CSIT | -7.70332 | 114.0129 | Panji, Situbondo | |

model formed has fewer pixels, because only neighbouring pixels will be processed. In the vertical results (ascending, descending, and 2.5D model), the darker colours indicate greater subsidence, and lighter colours indicate less subsidence. In the EW direction, negative values denote westward movement, while positive values indicate eastward movement.

Figure 5 clearly shows the distribution of land subsidence in *pantura*. To analyze the distribution further, cross-section lines were created across coastal cities, as shown in Figure 6. The corresponding land subsidence rates in cm/year are summarized in Table 3.

A further analysis shows that the largest subsidence rates in the vertical ascending and vertical descending have different values. This discrepancy may occur due to various factors, such as differences in orbit paths, differences in topography variations, threshold settings, and interferogram quality. The use of a 2.5D model helps address these discrepancies.

The results indicate that three regencies or cities with land subsidence exceeding 100 mm are: Pekalongan Regency by -137.94 mm/year, Semarang City by 144.34 mm/year, and Demak Regency by -146.45 mm/year. According to Ardha *et al*. (2021), land subsidence rates in Jakarta resulted at 80 mm/year, Cirebon at -20 mm/year, Pekalongan at -110.2 mm/year, Semarang at -60 mm/year, and Surabaya at -40.3 mm/year.

The findings of previous studies with the current results suggests that land subsidence consistently occurred in Jakarta, Cirebon, Pekalongan, Semarang, and Demak. However, the exact subsidence values differ due to the variations in the InSAR method, the number of observations, the time span, and the processing techniques used.

## Subsidence Locations

*a. Subsidence in Serang City*

Serang City, the capital of Banten Province, plays as administrative functions and an economic centre such as a centre for trade, services, and industry. Its role is very crucial for the development of the surrounding urban areas. Figures 7 and 8 show that the highest subsidence occurs in the centre of Serang City. This finding indicates that subsidence in Serang City occurs predominantly in dense residential areas and rice fields.

*b. Subsidence in Tangerang City, Tangerang Regency, Jakarta, Bekasi City, and Bekasi Regency*

The Jabodetabek (Greater Jakarta) area encompassing Tangerang City, Tangerang Regency, Jakarta, Bekasi Regency, and Bekasi City, is one of the largest metropolitan areas in Indonesia. r Jakarta Province serves as the hub for government, business, finance, and other sectors.

To the west of Jakarta Province, Tangerang City has developed rapidly as a hub for industry and trade, while Tangerang Regency hosts various industrial and residential areas. To the east, The Bekasi Regency has experienced growth in industrial and residential sectors, and Bekasi City also

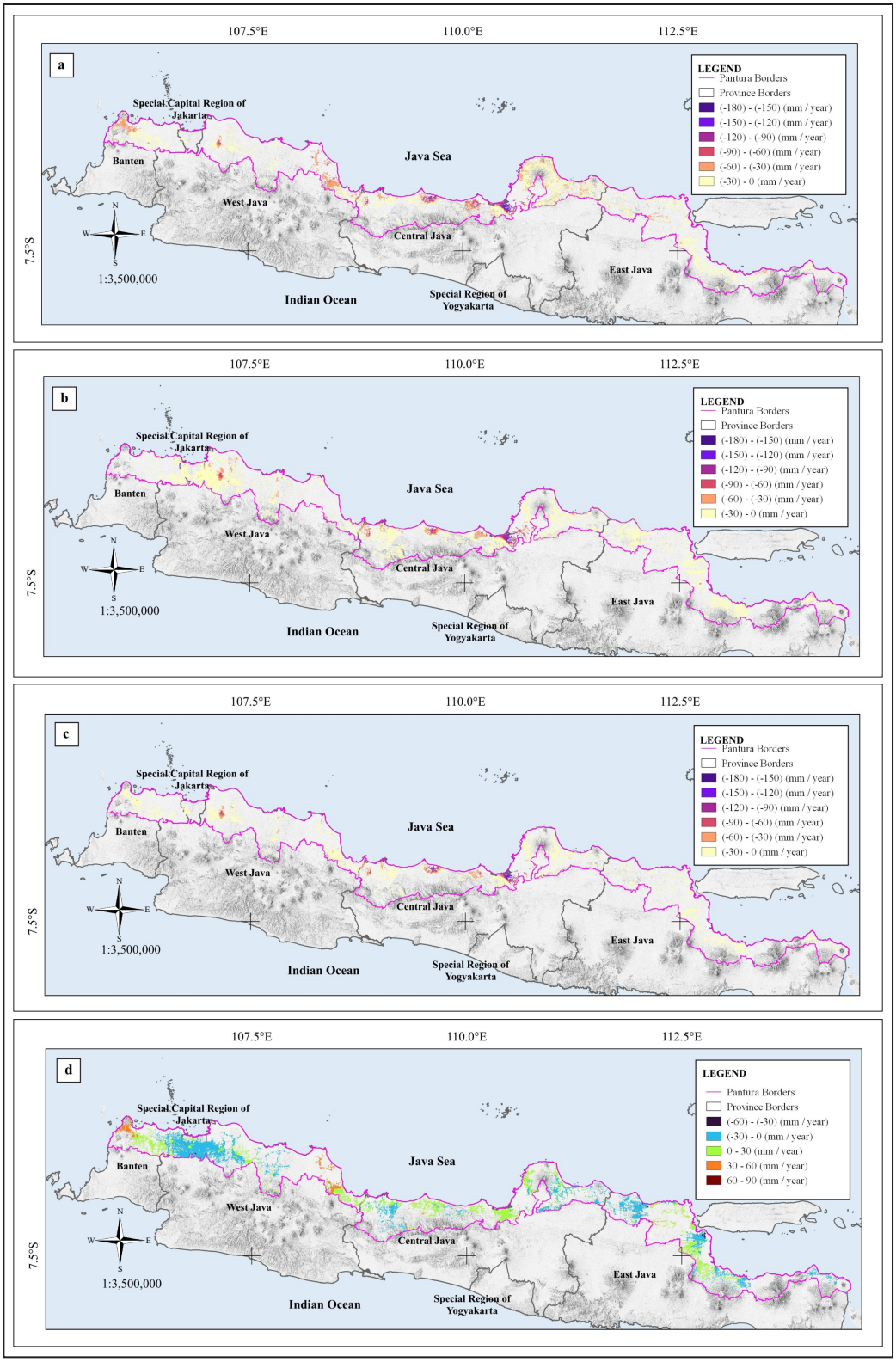


Figure 5. Distribution of land subsidence in *pantura*. (a) vertical ascending; (b) vertical descending; (c) 2.5D model in the UD direction; and (d) 2.5D model in the EW direction.

becoming a major economic and social activity in Greater Jakarta area. With a growing population and evolving infrastructure, The Greater Jakarta area continues to be a major focus for Indonesia

Table 3. Maximum Subsidence Value on The Line(C) 2.5D model in the UD direction, and (D) 2.5D model in the EW direction

| Location | Figure | Line | Vertikal Asc (mm/year) | Vertikal Des (mm/year) | UD (mm/year) | EW (mm/year) | High UD (mm/year) |
|---|---|---|---|---|---|---|---|
| Serang City | a | Line A-A' | -84.33 | -48.06 | -67.26 | 19.66 to 31.41 | - 67.26 |
| Special Capital Region of Jakarta | b | Line A-A' | -44.31 | -57.86 | -42.11 | -0.61 to 6.17 | - 42.11 |
| | | Line B-B' | -19.58 | -25.92 | -23.15 | -18.6 to -3.91 | |
| Tangerang City | | Line C-C' | -9.34 | -28.04 | -18.82 | -21.05 to -10.36 | -18.86 |
| Bekasi City | | Line D-D' | -0.10 | -23.77 | -13.01 | -21.98 to -14.44 | - 13.01 |
| Bekasi Regency | | Line E-E' | -17.12 | -26.00 | -19.52 | -21.54 to 1.54 | - 93.33 |
| | | Line F-F' | -89.86 | -95.69 | -93.33 | -15.35 to 2.42 | |
| | | Line G-G' | -30.81 | -78.70 | -58.11 | -32.99 to -8.9 | |
| Cirebon City and Cirebon Regency | c | Line A-A' | -75.37 | -12.18 | -39.27 | 21.6 to 44.34 | - 17.50 and - 39.27 |
| Cirebon Regency | | Line B-B' | -49.45 | -27.78 | -35.22 | -3.39 to 17.07 | - |
| Brebes Regency | d | Line A-A' | -63.84 | -47.54 | -54.79 | 2.51 to 10.64 | - 82.25 |
| | | Line B-B' | -85.21 | -79.63 | -82.25 | -2.28 to 7.11 | |
| | | Line C-C' | -51.60 | -66.31 | -54.37 | -4.16 to 7.36 | |
| Tegal City | | Line D-D' | -34.48 | -33.34 | -32.98 | -6.6 to 8.19 | - 30.64 |
| Tegal Regency | | Line E-E' | -38.67 | -34.97 | -34.62 | -3.97 to 6.08 | - 34.62 |
| Pemalang Regency and Pekalongan City | e | Line A-A' | -115.62 | -92.55 | -112.37 | 0.81 to 16.56 | - 79.46 and - 95.55 |
| | | Line B-B' | -105.10 | -99.29 | -108.11 | -10.35 to 19.32 | |
| Pekalongan Regency | | Line C-C' | -133.38 | -116.35 | -137.94 | -0.74 to 20.21 | - 137.94 |
| Kendal Regency | f | Line A-A' | -100.69 | -55.23 | -64.39 | 8.24 to 20.81 | - 64.39 |
| | | Line B-B' | -83.56 | -44.37 | -61.61 | 12.27 to 24.78 | |
| Semarang City and Demak Regency | | Line C-C' | -122.98 | -108.51 | -114.18 | -2.55 to 10.3 | - 144.34 and - 146.45 |
| | | Line D-D' | -172.03 | -136.08 | -146.45 | -0.78 to 20.2 | |
| Demak Regency | | Line E-E' | -144.28 | -126.19 | -132.78 | -5.19 to 12.3 | - |
| Gresik Regency | g | Line A-A' | -116,23 | -59,41 | -61,47 | 26,41 | - 61.47 |

economic development and growth. Figure 9 show land subsidence in:

- Residential area in Tangerang Regency and Bekasi Regency (Figures 9a, e)
- Dense residential area Tangerang City (Figure 9b)
- Dense residential area and secondary forest mangrove in Jakarta (Figure 9c)
- Residential areas adjacent to the river flow Bekasi City (Figure 9d).
- Residential areas and rice field adjacent to the river flow Bekasi Regency (Figure 9f).

According to Takagi *et al*. (2016), land subsidence plays an important role in expanding coastal flooding-prone area in Jakarta until 2050. The study predicted that flooding would extend several kilometers inland from Jakarta's north coast by combining the effects of abnormal high tides, sea level rise, and land subsidence within a hydrodynamic model (Takagi *et al*., 2016).

c. *Subsidence in Cirebon City and Cirebon Regency*

Cirebon City and Cirebon Regency, key economic hubs in West Java Province, are vital for trade, distribution agriculture and fisheries sectors to support economic growth. Figure 10 shows land subsidence affecting Cirebon City and Cirebon Regency. Figure 10 also shows land subsidence in:

- Residential area and rice fields in Cirebon Regency (Figure 10a)
- Dense residential area in Cirebon Ciy (Figure 10b)

In addition to land subsidence, there is also accretion along the Cirebon coast. A research by Pratama *et al*. (2023) using Landsat data revealed an increase in coastal area by 1,468.88 ha from 1978 to 2018. Moreover, Triana *et al*. (2023) reported that Cirebon experienced erosion reaching -21.9 km (35.6 %) and accretion of +39.6 km

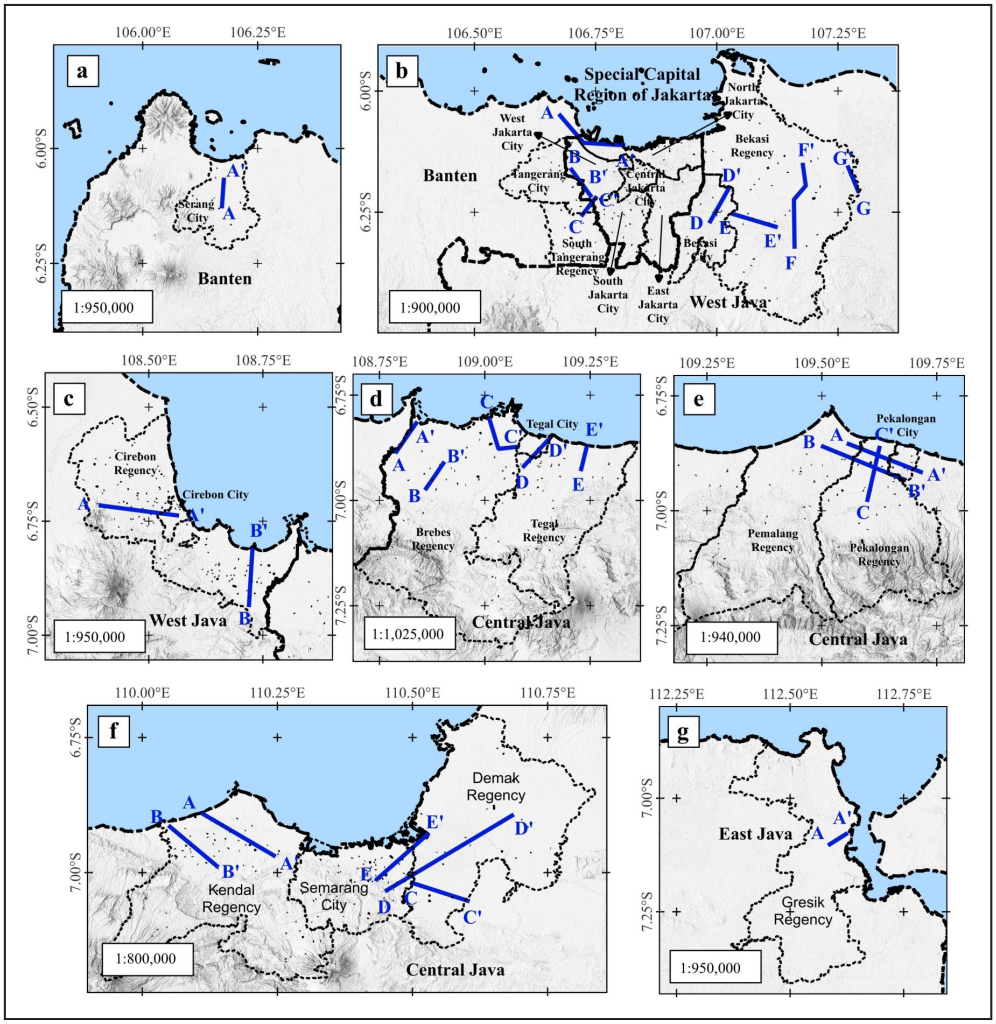


Figure 6. Identification of land subsidence value in Pantura major cities. (a) Serang City; (b) Tangerang City, South Tangerang Regency, Jakarta, Bekasi City, Bekasi Regency; (c) Cirebon Regency, Cirebon City; (d) Brebes Regency, Tegal City, Tegal Regency; (e) Pemalang Regency, Pekalongan City, Pekalongan Regency; (f) Kendal Regency, Semarang City, Demak Regency; and (g) Gresik Regency.

(64.4 %) along its 73.16 km coastline between 2000 and 2020. The study also predicts that by 2050, coastal flooding could impact ponds, settlements, agricultural land, markets, and mangrove forests along the Cirebon coast due to combined effects of sea level rise, land subsidence, and extreme wave events. Continuous erosion, accretion, and subsidence could contribute significantly to future tidal flooding risks, as emphasized in Triana *et al*. (2023).

*d. Subsidence in Brebes Regency, Tegal Regency, and Tegal City*

Brebes Regency, Tegal Regency, and Tegal City, located in Central Java Province, posses diverse economic sectors, ranging from agriculture, plantations, to trade, industry, and services. Figures 11 and 12 show land subsidence in:

- Residential areas and rice fields adjacent to the river flow in Brebes Regency (Figure 12a)
- Dense residential areas in Tegal City (Figure 12b), with a higher intensity approaching the north coast of Java.
- Residential areas, dryland agiculture, and rice fields of Tegal Regency (Figure 12c) that followed the road network along the north coast of Java.

In line with land subsidence, Brebes Regency also experienced significant coastline change. A research by Nguyen and Takewaka (2020) reveals

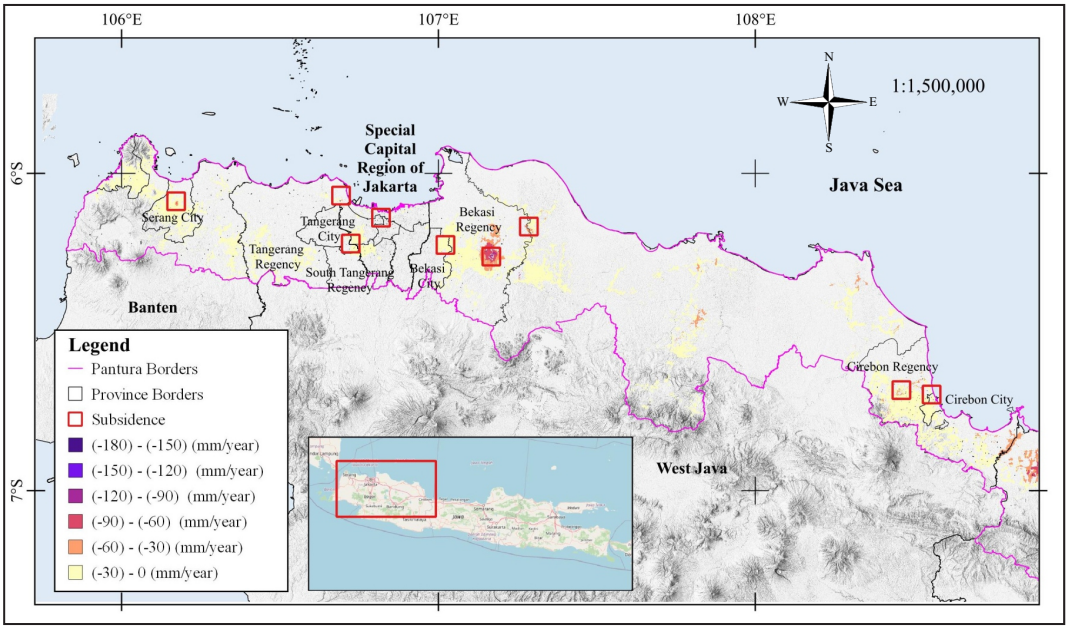


Figure 7. Identification of location subsidence in Banten, Jakarta, and West Java Provinces.

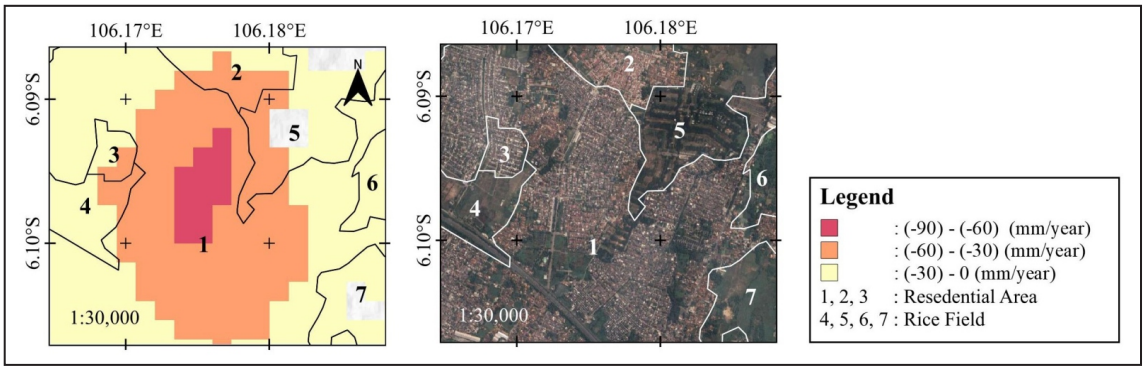


Figure 8. Highest land subsidence (left) and land use overlay with image (right) in Serang City.

that land subsidence significantly worsen shoreline change. If subsidence continues, it could exacerbate various coastal issues in Brebes and Tegal Regency.

*e. Subsidence in Pemalang Regency, Pekalongan Regency, and Pekalongan City*

Pemalang Regency, Pekalongan Regency, and Pekalongan City, located in Central Java Province, have diverse economic characteristics, particularly strong in trade, fisheries, and *batik* industry (as the icon of Pekalongan). Figure 13 shows land subsidence in these regions, with focused on:

- Residential areas and rice field that follow road and river networks (13a) of Pemalang Regency,
- The same conditions of Pekalongan Regency (13b),
- Residential areas adjacent to the river flow in Pekalongan City (13c)

Severe coastal abrasion of up to 232 m between 1988 and 2021 was recorded in high-subsidence areas, according to Chulafak *et al.* (2022). This abrasion has resulted in various coastal land lost like previous areas.

*f. Subsidence in Kendal Regency, Semarang City, and Demak Regency*

Kendal Regency, Semarang City, and Demak Regency are cities in The Central Java Province. Semarang City, the capital, is the third most popu-

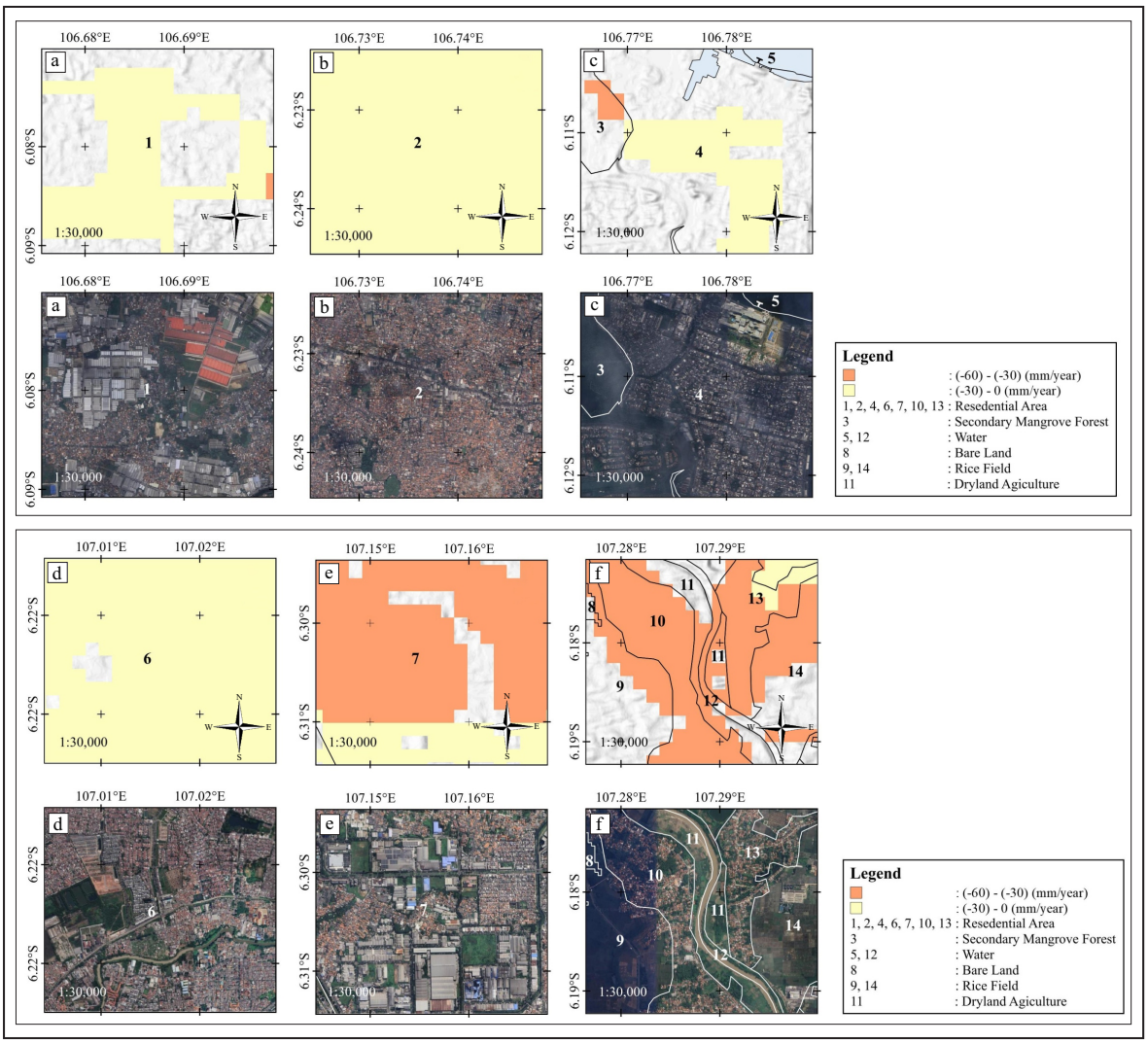


Figure 9. Highest land subsidence (top) and land use overlay with image (bottom). (a) Tangerang Regency; (b) Tangerang City; (c) Jakarta; (d) Bekasi City; and (e,f) Bekasi Regency.

lous city along the north coast of Java after Jakarta and Surabaya, with significant activity in trade, industry, and services. Kendal and Demak regencies focus more on agriculture, fisheries, and new industries. Figure 14 shows land subsidence in:

- Residential areas, rice fields, and dryland agriculture that follow the road network in Kendal Regency (14a),
- Dense residential area in Semarang Ciy (14b),
- Residential areas and rice fields in Demak Regency (14c).

Land subsidence in Semarang City exacerbates the annual challenge of coastal flooding. A recent study identified high vulnerability in subdistricts such as Genuk, Tugu, and northern Semarang (Setyaningsih *et al*., 2024). Additionally, severe erosion and coastline changes in nearby areas like Sayung (Demak District) and Sriwulan Villages increase the risk of environmental damage, making these coastal regions highly susceptible to combined impacts of subsidence, flooding, and shoreline retreat (Muskananfola *et al*., 2020).

*g. Subsidence in Gresik Regency*

Gresik Regency, a city in East Java Province, plays a very important role in regional economic development due to their industrial and trade activities. Figure 15 identifies residential areas as the primary zones affected by subsidence.

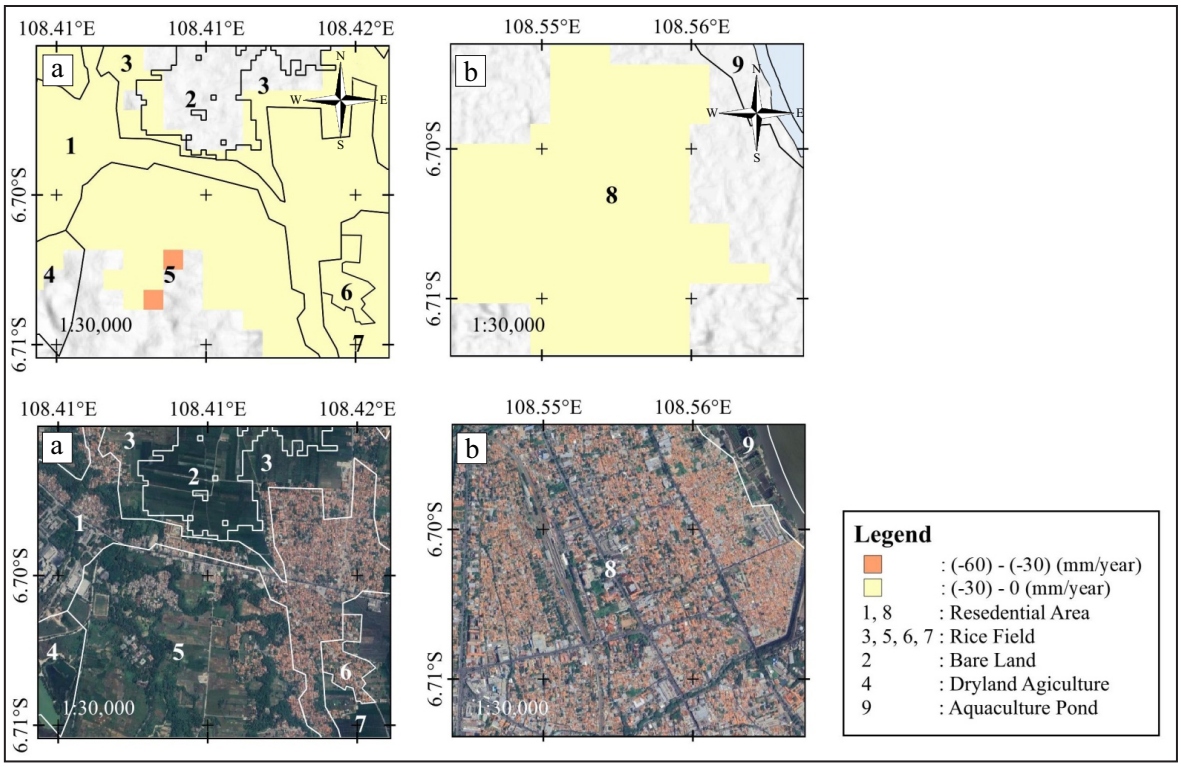


Figure 10. Highest land subsidence (top) and land use overlay with image (bottom). (a) Cirebon Regency and; (b) Cirebon City.

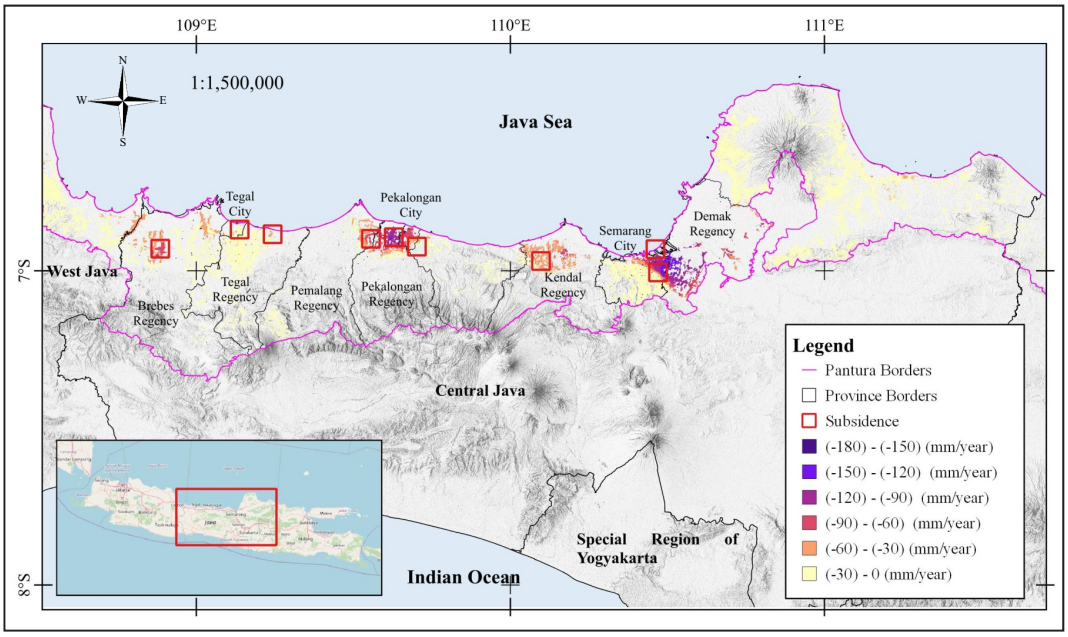


Figure 11. Identification of location subsidence in Central Java Province.

Meanwhile, shoreline changes due to sediment deposition from The Bengawan Solo River have resulted in more accretion than erosion (Prasita *et al*., 2023).

## Validation Velocity with CORS

There are twenty CORS observation stations spread along the north coast of Jawa. However, only twelve stations were used in this study

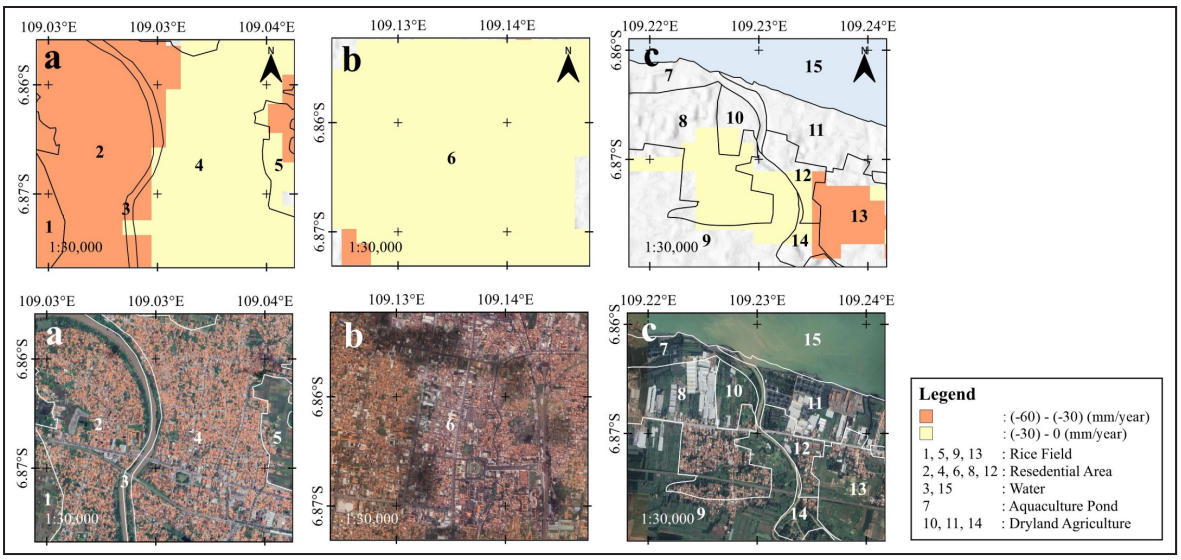


Figure 12. Highest land subsidence (top) and land use overlay with image (bottom). (a) Brebes Regency; (b) Tegal Regency; and (c) Tegal City.

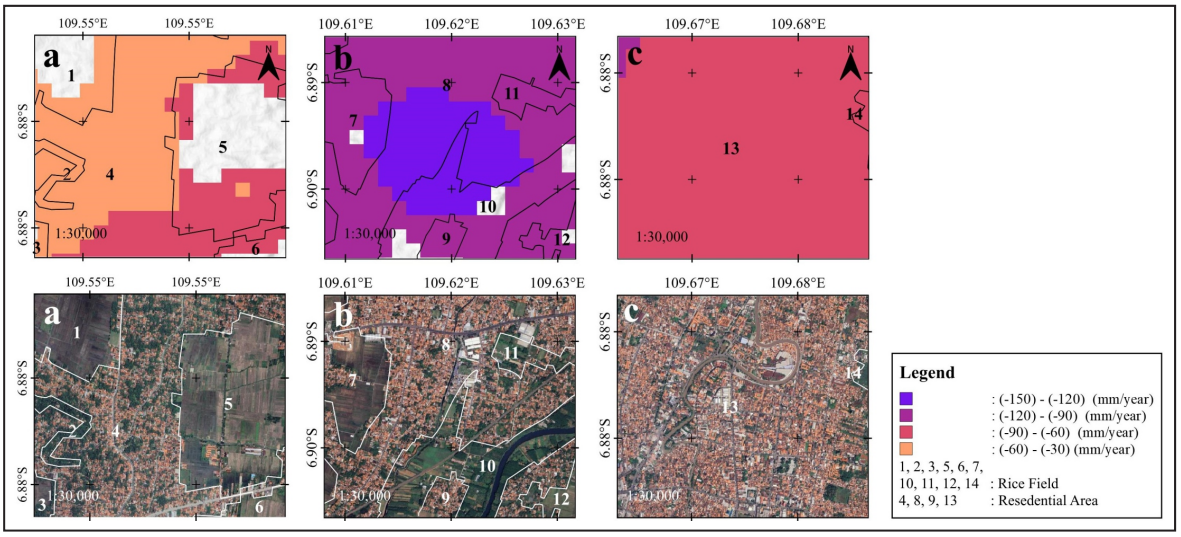


Figure 13. Highest land subsidence (top) and land use overlay with image (bottom). (a) Pemalang Regency; (b) Pekalongan Regency; and (c) Pekalongan City.

due to the absence of pixels from the LiCSBAS processing.

Table 4 compares the standard deviations of LiCSBAS and CORS processing results. The standard deviation values for LICSBAS 1D are more varied than those for CORS 1D. Meanwhile, in the 2.5D model, the standard deviation in the EW direction is smaller than in the UD direction indicating higher accuracy for the 2.5D UD model.

Table 5 and Table 6 summarize the differences in velocity values between LiCSBAS and CORS. The variations range from 0.41 mm/year to 50.98 mm/year for vertical ascending and descending orbits and from 0.85 to 48.91 mm/year for 2.5D UD and EW models. The 2.5D UD model demonstrates improved accuracy by integrating ascending and descending data.

The RMSE values for the vertical ascending, descending, UD, and EW directions (Table 7) range from fractions of a millimeter to centimeters, with the 2.5D UD model achieving the smallest values, indicating higher accuracy. The

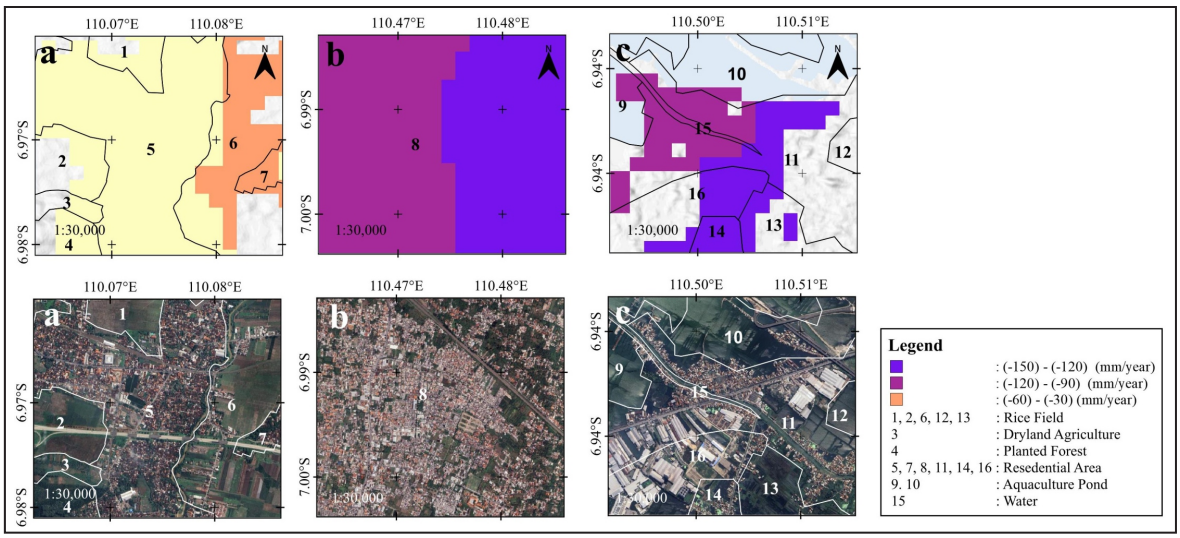


Figure 14. Highest land subsidence (top) and land use overlay with image (bottom). (a) Kendal Regency; (b) Semarang City; and (c) Demak Regency.

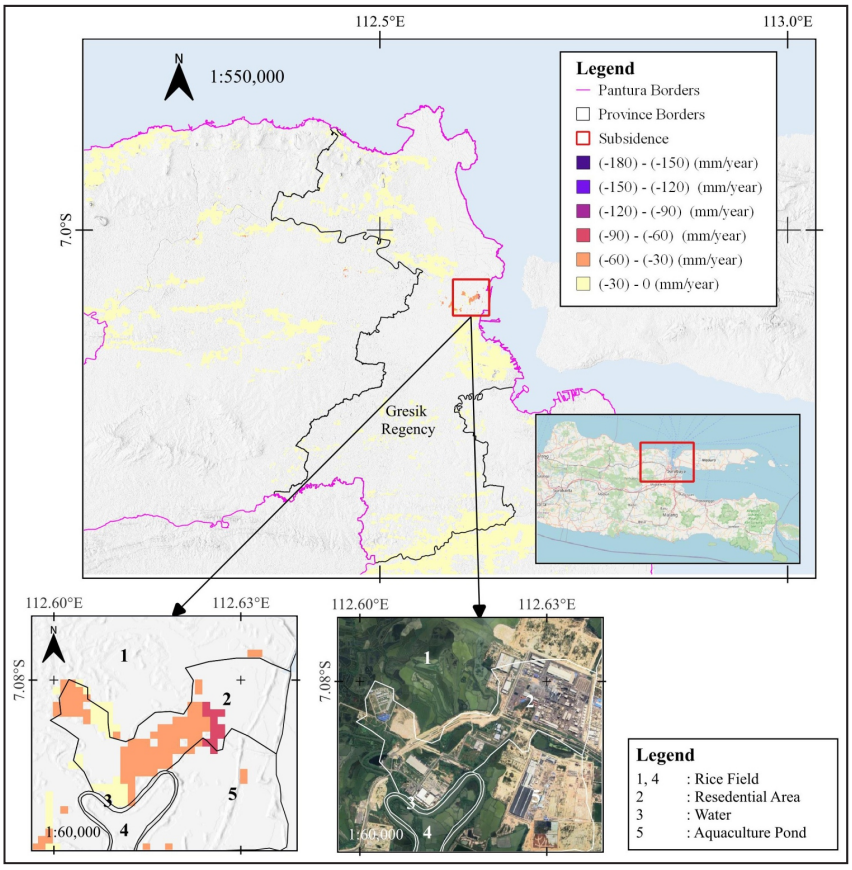


Figure 15. Land subsidence location in Gresik Regency.

2.5D UD model is recommended for monitoring vertical subsidence due to its ability to integrate data from multiple orbits. Meanwhile, EW displacement values are less using LiCSBAS, as it primarily focuses on vertical shifts. In contrast, GNSS CORS performs better in detecting horizontal shifts (EW/NS), as supported by its lower standard deviation values for horizontal displace-

Table 4. Standard Deviation of LiCSBAS Processing Results

| Name | LiCSBAS | | CORS | | | |
|---|---|---|---|---|---|---|
| | 1D | | 1D | | 2.5D Model | |
| | σAsc (mm) | σDes (mm) | σUD Asc (mm) | σUD Asc (mm) | σEW (mm) | σUD (mm) |
| CBTU | 3.74 | 2.57 | 0.65 | 0.79 | 0.17 | 0.50 |
| CGON | 2.89 | 1.45 | 2.53 | 3.39 | 0.20 | 2.02 |
| CLMG | 3.05 | 1.82 | 0.78 | 1.39 | 0.19 | 0.69 |
| CMJT | 1.77 | 1.22 | 2.24 | 1.59 | 0.22 | 1.59 |
| CPAS | 2.30 | 1.52 | 2.36 | 1.39 | 0.49 | 1.35 |
| CPKL | 3.04 | 0.49 | 1.34 | 1.07 | 0.16 | 0.83 |
| CPWD | 4.12 | 2.02 | 2.26 | 1.98 | 0.20 | 1.51 |
| CSBY | 0.68 | 0.38 | 0.90 | 1.19 | 0.20 | 0.71 |
| CSEM | 2.01 | 2.02 | 0.92 | 0.95 | 0.19 | 0.66 |
| CSIT | 1.86 | 2.19 | 0.86 | 1.04 | 0.22 | 0.69 |
| CTBN | 2.22 | 2.18 | 0.86 | 1.31 | 0.21 | 0.72 |
| CTGL | 1.16 | 1.14 | 1.06 | 1.20 | 0.28 | 0.81 |

Table 5. Difference in Velocity Values between LiCSBAS and CORS in Vertical Ascending And Vertical Descending

| Name | Ascending (UD) (mm) | | | Descending (UD) (mm) | | |
|---|---|---|---|---|---|---|
| | LiCSBAS | CORS | Difference | LiCSBAS | CORS | Difference |
| CBTU | 10.72 | 0.44 | 10.28 | 0.11 | 0.32 | 0.21 |
| CGON | -39.53 | -19.51 | 20.07 | 26.06 | -24.92 | 50.98 |
| CLMG | -28.63 | -5.56 | 23.07 | -2.28 | -7.31 | 5.03 |
| CMJT | -19.29 | -1.82 | 17.47 | 6.79 | -11.5 | 18.29 |
| CPAS | 11.66 | -5.19 | 16.85 | -0.45 | -9.53 | 9.08 |
| CPKL | -84.87 | -90.38 | 5.51 | -61.89 | -92.02 | 30.13 |
| CPWD | -10.40 | -39.37 | 28.97 | -15.11 | -18.48 | 3.37 |
| CSBY | 2.90 | 2.49 | 0.41 | -1.59 | -2.15 | 0.56 |
| CSEM | -15.69 | -5.61 | 10.08 | -3.75 | -0.95 | 2.8 |
| CSIT | -0.54 | 3.43 | 3.97 | -19.54 | -1.56 | 17.98 |
| CTBN | 25.29 | -3.77 | 29.09 | -14.74 | -0.46 | 14.28 |
| CTGL | -29.26 | -19.94 | 9.32 | -18.69 | -17.49 | 1.20 |

Table 6 .The Difference in Velocity Values between LiCSBAS And CORS in 2.5D Model UD And EW

| Name | 2.5D Model (UD) (mm) | | | 2.5D Model (EW) (mm) | | |
|---|---|---|---|---|---|---|
| | LiCSBAS | CORS | Difference | LiCSBAS | CORS | Difference |
| CBTU | 4.51 | 0.39 | 4.11 | -7.1 | 24.32 | 31.42 |
| CGON | -8.14 | -21.24 | 13.1 | 43.69 | 24 | 19.37 |
| CLMG | -15.25 | -5.99 | 9.26 | 16.94 | 25.55 | 8.61 |
| CMJT | -5.79 | -3.98 | 1.80 | 17.67 | 26.16 | 8.49 |
| CPAS | 5.23 | -7.59 | 12.82 | -8.48 | 27.24 | 35.72 |
| CPKL | -80.01 | -91.66 | 11.65 | 10.45 | 23.67 | 13.22 |
| CPWD | -12.77 | -23.74 | 10.97 | -4.34 | 25.37 | 29.71 |
| CSBY | 0.58 | 1.43 | 0.85 | -3.28 | 26.34 | 29.62 |
| CSEM | -10.7 | -2.58 | 8.12 | 8.75 | 23.63 | 14.886 |
| CSIT | -11.67 | 1.48 | 13.15 | -11.44 | 26.57 | 38.01 |
| CTBN | 5.36 | -2.25 | 7.61 | -23.82 | 25.09 | 48.91 |
| CTGL | -21.70 | -18.7 | 3.00 | 7.25 | 21.92 | 14.67 |

Table 7. RMSE Values from LiCSBAS And CORS Processing Results

| Parameter | RMSE (mm) | | | |
|---|---|---|---|---|
| | 1D | | 2.5D | |
| | Vertical Ascending | Vertical Descending | UD | EW |
| Velocity | 16.5 | 18.6 | 8.8 | 26.3 |

ment. The results of this study are consistent with research conducted by Janur (2024).

## Conclusions

A 2.5D modelling approach is more robust for observing subsidence than using only ascending or descending orbits. This increased robustness is due not only to the use of two different orbit observations, but also to the ability to capture both vertical and horizontal displacements. Based on the 2.5D model, the UD direction shows the highest rates of land subsidence in the following areas: Demak Regency at 146.45 mm/year, Semarang City at 144.34 mm/year, and Pekalongan Regency at 137.94 mm/year. Land subsidence is not evenly distributed throughout the region, but it is concentrated at several points, particularly in dense residential areas and rice fields. In Pekalongan Regency, the highest subsidence occurs about 6 km from the coastline, in Semarang City about 5 km, and in Demak Regency directly on the coastline. In addition, these three areas of land subsidence are also located in Alluvium Formations, which are more easily compressed, and thus more susceptible to subsidence. Therefore, areas close to the coastline with Alluvium Formations and intensive land use are greater risk of subsidence than other areas.

An accuracy assessment using twelve CORS stations showed RMSE values ranging from millimeters to centimeters. The RMSE value for ascending vertical is 16.5 mm, for descending vertical is 18.6 mm, for UD is 8.8 mm, and for EW is 26.3 mm. It can be seen that the RMSE value of UD provides the best results compared to vertical ascending and vertical descending measurement in observing subsidence. While EW displacement from LiCSBAS generally showed lower accuracy due to its sensitivity to vertical movements. In some cases, it achieved higher precision.

## Acknowledgements

The authors extend their gratitude to the reviewers for their valuable comments, which have greatly enhanced the quality of this article. We also gratefully acknowledge the European Space Agency (ESA) for providing Sentinel-1 data. Special thanks are given to LiCSBAS for providing the tools and software essential for InSAR data processing, as well as to The Badan Informasi Geospasial (BIG) for supplying the CORS data. The successful completion of this research was made possible through the cooperation and support of all these contributors. This publication is part of Janur's thesis research (Janur, 2024), conducted at The Department of Geodetic Engineering, Faculty of Engineering, Universitas Gadjah Mada.

## References

Anjasmara, I.M., Yulyta, S.A., and Taufik, M., 2020. *Application of Time Series InSAR (SBAS) Method using Sentinel-1A Data for Land Subsidence Detection in Surabaya City*. 10 (1).

Ardha, M., Khomarudin, M.R., Pranowo, W.S., Chulafak, G.A., Yudhatama, D., Mujio, and Pravitasari, S., 2022. Spatial information on the rate of subsidence in North Coastal Area of Java and the estimation of inundation in 2031. *IOP Conference Series: Earth*

*and Environmental Science*, 1109 (1). DOI: 10.1088/1755-1315/1109/1/012022.

Bassols, J.B., Suñé, V.E., Crosetto, M., Barra, A., and Gerard, P., 2021. D-InSAR monitoring of ground deformation related to the dewatering of construction sites. A case study of Glòries Square, Barcelona. *Engineering Geology*, 286. DOI: 10.1016/j.enggeo.2021.106041.

Bramanto, B., Gumilar, I., Sidiq, T.P., Rahmawan, Y.A., and Abidin, H.Z., 2023. Geodetic evidence of land subsidence in Cirebon, Indonesia. *Remote Sensing Applications: Society and Environment*, 30. DOI: 10.1016/j.rsase.2023.100933.

Castañeda, C., Pourthié, N., and Souyris, J.C., 2011. Dedicated SAR interferometric analysis to detect subtle deformation in evaporite. *International Journal of Remote Sensing*, p.1-27. DOI: 10.1080/01431161003631584.

Chulafak, G.A., Khomarudin, M.R., Ardha, M., Pranowo, W., Prayudha, B., and Mujio, 2022. Thirty years of change of Pekalongan coastline based on Landsat imagery. *IOP Conference Series: Earth and Environmental Science*, 1109 (1). DOI: 10.1088/1755-1315/1109/1/012056.

Davydzenka, T., Tahmasebi, P., and Shokri, N., 2024. Unveiling the Global Extent of Land Subsidence: The Sinking Crisis. *Geophysical Research Letters*, 51 (4). DOI: 10.1029/2023GL104497.

Ding, X.L., Liu, G.X., Li, Z.W., Li, Z.L., and Chen. Y.Q., 2004. Ground Subsidence Monitoring in Hong Kong with Satellite SAR Interferometry. *Photogrammetric Engineering And Remote Sensing*, 70, p.1151-1156. DOI: 10.14358/PERS.70.10.1151.

Fuhrmann, T. and Garthwaite, M., 2019. Resolving three-dimensional surface motion with InSAR: Constraints from multi-geometry data fusion. *Remote Sensing*, 11 (3). DOI: 10.3390/rs11030241.

Fujiwara, S., Nishimura, T., Murakami, M., Nakagawa, H., Tobita, M., and Rosen, P.A., 2000. 2.5-D surface deformation of M6.1 earthquake near Mt Iwate detected by SAR interferometry. *Geophysical Research Letters*, 27 (14), p.2049-2052. DOI: 10.1029/1999GL011291.

Galloway, D.L. and Burbey, T.J., 2011. Review: Regional land subsidence accompanying groundwater extraction. *Hydrogeology Journal*, 19 (8), p.1459-1486. DOI: 10.1007/s10040-011-0775-5.

Gavkosh, M.B., Hosseini, S.M., Ashtiani, B.A., Sohani, Y., Ebrahimian, H., Morovat, F., and Ashrafi, S., 2021. Land subsidence: A global challenge. *Science of the Total Environment*, 778. DOI: 10.1016/j.scitotenv.2021.146193.

Geng, J., Chen, X., Pan, Y., Mao, S., Li, C., Zhou, J., and Zhang, K., 2019. PRIDE PPP-AR: an open-source software for GPS PPP ambiguity resolution. *GPS Solutions*, 23 (4). DOI: 10.1007/s10291-019-0888-1.

Hammond, J.O.S., Wookey, J., Kaneshima, S., Inoue, H., Yamashina, T., and Harjadi, P., 2010. Systematic variation in anisotropy beneath the mantle wedge in the Java-Sumatra subduction system from shear-wave splitting. *Physics of the Earth and Planetary Interiors*, 178 (3-4), p.189-201. DOI: 10.1016/j.pepi.2009.10.003.

Harintaka, H., Suhadha, A.G., Syetiawan, A., Ardha, M., and Rarasati, A., 2024. Current land subsidence in Jakarta: a multi-track SBAS InSAR analysis during 2017-2022 using C-band SAR data. *Geocarto International*, 39 (1). DOI: 10.1080/10106049.2024.2364726.

Huning, L.S., Love, C.A., Anjileli, H., Vahedifard, F., Zhao, Y., Chaffe, P.L.B., Cooper, K., Alborzi, A., Pleitez, E., Martinez, A., Ashraf, S., Mallakpour, I., Moftakhari, H., and AghaKouchak, A., 2024. Global Land Subsidence: Impact of Climate Extremes and Human Activities. In *Reviews of Geophysics,* 62 (4). John Wiley and Sons Inc. DOI: 10.1029/2023RG000817.

Janur, A., 2024. Kajian Dan Pemodelan 2,5D Laju Penurunan Muka Tanah Dengan Metode Small Baseline Subset (SBAS) (Studi Kasus: Pantai Utara Jawa), Tesis, Magister Teknik Geomatika, Departemen Teknik Geodesi, Fakultas Teknik, Universitas Gadjah Mada].

https://etd.repository.ugm.ac.id/penelitian/detail/239343.

Lanari, R., Bonano, M., Casu, F., De Luca, C., Manunta, M., Manzo, M., Onorato, G., and Zinno, I., 2020. Automatic generation of Sentinel-1 continental scale DInSAR deformation time series through an extended P-SBAS processing pipeline in a cloud computing environment. *Remote Sensing*, 12 (18). DOI: 10.3390/RS12182961.

Metcalfe, I., 2011. Tectonic framework and Phanerozoic evolution of Sundaland. *Gondwana Research*, 19 (1), p.3-21. DOI: 10.1016/j.gr.2010.02.016.

Morishita, Y., Lazecky, M., Wright, T J., Weiss, J.R., Elliott, J.R., and Hooper, A., 2020. LiCSBAS: An open-source insar time series analysis package integrated with the LiCSAR automated sentinel-1 InSAR processor. *Remote Sensing*, 12 (3). DOI: 10.3390/rs12030424.

Muskananfola, M.R., Supriharyono, and Febrianto, S., 2020. Spatio-temporal analysis of shoreline change along the coast of Sayung Demak, Indonesia using Digital Shoreline Analysis System. *Regional Studies in Marine Science*, 34. DOI: 10.1016/j.rsma.2020.101060.

Nguyen, Q.H. and Takewaka, S., 2020. Land subsidence and its effects on coastal erosion in the Nam Dinh Coast (Vietnam). *Continental Shelf Research*, 207.DOI: 10.1016/j.csr. 2020. 104227.

Novico, F., Menier, D., Mathew, M., Ramkumar, M., Santosh, M., Endyana, C., Dewi, K.T., Kurniawan, I., Lambert, C., Goubert, E., and Hendarmawan, 2022. Impact of Late Quaternary climatic fluctuations on coastal systems: Evidence from high-resolution geophysical, sedimentological and geochronological data from the Java Island. *Marine and Petroleum Geology*, 136. DOI: 10.1016/j.marpetgeo.2021.105399.

Parwata, I.N.S., Osawa, T., and Abo, H., 2023. Land Subsidence Monitoring in Semarang (Indonesia) by SBAS-DInSAR using ALOS-2 and Sentinel-1 SAR data from 2015 to 2023. *APSAR 2023 - 2023 8th Asia-Pacific Conference on Synthetic Aperture Radar*. DOI: 10.1109/APSAR58496.2023.10388880.

Pasari, S., Simanjuntak, A.V.H., Mehta, A., Neha, and Sharma, Y., 2021. The Current State of Earthquake Potential on Java Island, Indonesia. *Pure and Applied Geophysics*, 178 (8), p.2789-2806.DOI: 10.1007/s00024-021-02781-4.

Pratama, R.Y., Sulaksana, N., Sukiyah, E., Iskandarsyah, T.Y.W.M., Novico, F., Zulfahmi, Z., Sudjono, E. H., and Ranawijaya, D., 2023. Short-Term Coastal Landscape Evolution In Cirebon Bay Using Coastline Environment Analysis. *Journal of Environmental Engineering and Landscape Management*, 31 (3), p.186-195. DOI: 10.3846/jeelm.2023.19468.

Prasita, V.D., Bintoro, R.S., Nurmalia, I., Widagdo, S., Rosana, N., and Sugianto, E., 2023. The Coastline Change Pattern of Gresik Beach around the Madura Strait, Indonesia. *Indonesian Journal of Geography*, 55 (3), p.527-537. DOI: 10.22146/ijg.80934.

Ren, C., Shi, X., Li, X., and Zhang, Z., 2019. *Land Subsidence Monitoring in Nanning Based on Sentinel-1A data and SBAS-InSAR*. p.1-4. DOI: 10.1109/APSAR46974. 2019.9048363.

Sarah, D., Hutasoit, L.M., Delinom, R.M., and Sadisun, I.A., 2020. Natural Compaction of Semarang-Demak Alluvial Plain and Its Relationship to the Present Land Subsidence. *Indonesian Journal on Geoscience*, 7 (3), p.273-289. DOI: 10.17014/ijog.7.3.273-289.

Sarah, D., Soebowo, E., and Satriyo, N.A., 2021. Review of the land subsidence hazard in pekalongan delta, central java: Insights from the subsurface. *Rudarsko Geolosko Naftni Zbornik*, 36 (4), p.163-176.DOI: 10.17794/rgn.2021.4.13.

Schlüter, H.U., Gaedicke, C., Roeser, H.A., Schreckenberger, B., Meyer, H., Reichert, C., Djajadihardja, Y., and Prexl, A., 2002. Tectonic features of the southern Sumatra-western Java forearc of Indonesia. *Tectonics*, 21 (5), 11-1-11-15. DOI: 10.1029/2001TC901048.

Setyaningsih, W., Saputro, P.A., Indrayati, A., Kurniawan, E., Syifauddin, M., Wijaya, V., and Mahat, H., 2024. Spatial-Temporal

Distribution and Vulnerability Level of Tidal Flooding in the Coastal City of Semarang. *International Journal of Safety and Security Engineering*, 14 (05), p.1607-1615. DOI: 10.18280/ijsse.140527.

Suhadha, A.G. and Harintaka, H., 2024. Multi-dimensional displacement analysis of Semeru Volcano, Indonesia following December 2021 eruption from multitrack InSAR observation. *Earth Science Informatics*, 17 (2), p.1539-1552. DOI: 10.1007/s12145-024-01248-z.

Suroso, D.S.A. and Firman, T., 2018. The role of spatial planning in reducing exposure towards impacts of global sea level rise case study: Northern coast of Java, Indonesia. *Ocean and Coastal Management*, 153, p.84-97. DOI: 10.1016/j.ocecoaman.2017.12.007.

Susilo, S., Salman, R., Hermawan, W., Widyaningrum, R., Wibowo, S.T., Lumban-Gaol, Y.A., Meilano, I., and Yun, S.H., 2023. GNSS land subsidence observations along the northern coastline of Java, Indonesia. *Scientific Data*, 10 (1). DOI: 10.1038/s41597-023-02274-0.

Takagi, H., Esteban, M., Mikami, T., and Fujii, D., 2016. Projection of coastal floods in 2050 Jakarta. *Urban Climate*, 17, p.135-145. DOI: 10.1016/j.uclim.2016.05.003.

Takami, J., 2021. Land Subsidence Monitoring by SBAS-InSAR Technique with the Conversion to Horizontal-Vertical Displacements in Semarang. *Proceedings - 2021, 7th Asia-Pacific Conference on Synthetic Aperture Radar, APSAR 2021*. DOI: 10.1109/APSAR52370.2021.9688411.

Triana, K., Solihuddin, T., Husrin, S., Risandi, J., Mustikasari, E., Kepel, T.L., Salim, H.L., Sudirman, N., Prasetyo, A.T., and Helmi, M., 2023. An integrated satellite characterization and hydrodynamic study in assessing coastal dynamics in Cirebon, West Java. *Regional Studies in Marine Science*, 65. DOI: 10.1016/j.rsma.2023.103107.

Widada, S., Zainuri, M., Yulianto, G., Satriadi, A., and Wijaya, Y.J., 2020. Estimation of Land Subsidence Using Sentinel Image Analysis and Its Relation to Subsurface Lithology Based on Resistivity Data in the Coastal Area of Semarang City, Indonesia. *Journal of Ecological Engineering*, 21 (8), p.47-56. DOI: 10.12911/22998993/127394.

Wu, P.C., Wei, M., and D'Hondt, S., 2022. Subsidence in Coastal Cities Throughout the World Observed by InSAR. *Geophysical Research Letters*, 49 (7). DOI: 10.1029/2022GL098477

Wu, Z., Ma, P., Zheng, Y., Gu, F., Liu, L., and Lin, H., 2023. Automatic detection and classification of land subsidence in deltaic metropolitan areas using distributed scatterer InSAR and Oriented R-CNN. *Remote Sensing of Environment*, 290. DOI: 10.1016/j.rse.2023.113545.

Yulianto, F., Wibowo, M., Yananto, A., Perdana, D.H. .F., Wiguna, E.A., Prabowo, Y., Rahili, N., Nurwijayanti, A., Iswari, M.Y., Ratnasari, E., Rusdiutomo, A., Nugroho, S., Purwoko, A.S., Aziz, H., and Fachrudin, I., 2023. Coastal vulnerability assessment using the machine learning tree-based algorithms modeling in the north coast of Java, Indonesia. *Earth Science Informatics*, 16 (4), p.3981-4008. DOI: 10.1007/s12145-023-01135-z.

Zhang, P., Qian, X., Guo, S., Wang, B., Xia, J., and Zheng, X., 2023. A New Method for Continuous Track Monitoring in Regions of Differential Land Subsidence Rate Using the Integration of PS-InSAR and SBAS-InSAR. *Remote Sensing*, 15 (13). DOI: 10.3390/rs15133298.